On OH line formation and oxygen abundances in metal-poor stars

Martin Asplund and Ana Elia García Pérez

Astronomiska Observatoriet, Box 515, SE-751 20 Uppsala, Sweden
e-mail: martin@astro.uu.se, aegp@astro.uu.se

Abstract. The formation of the UV OH spectral lines has been investigated for a range of stellar parameters in the light of 3D hydrodynamical model atmospheres. The low atmospheric temperatures encountered at low metallicities compared with the radiative equilibrium values enforced in classical 1D hydrostatic model atmospheres have a profound impact on the OH line strengths. As a consequence, the derived O abundances using 3D models are found to be systematically lower by more than 0.6 dex at [Fe/H] $= -3.0$ compared with previous 1D analyses, casting doubts on the recent claims for a monotonic increase in [O/Fe] towards lower metallicities. In fact, taken at face value the resulting 3D LTE trend is in rough agreement with the conventional [O/Fe] plateau. Caution must, however, be exercised in view of the remaining assumptions in the 3D calculations. We have verified that the stellar parameters remain essentially unchanged with 3D model atmospheres provided that the infrared flux method ($\Delta T_{\rm eff} \lesssim 20$ K), Hipparcos parallaxes ($\Delta \log g \lesssim 0.05$) and Fe II lines ($\Delta$[Fe/H] $\lesssim 0.1$ dex) are utilised, leaving the 3D O abundances from OH lines largely intact (Δ[O/H] $\lesssim 0.05$ dex). Greater concern stems from possible departures from LTE in both the line formation and the molecular equilibrium, which, if present, would increase the derived O abundances again. Non-LTE line formation calculations with 1D model atmospheres suggest no significant steepening of the [O/Fe] trend even if the abundance corrections amount to about 0.2 dex for all investigated stellar parameters. We note, however, that the 3D case may not necessarily be as metallicity-independent. The apparent lack of laboratory or theoretical rate coefficients at the relevant temperatures for the involved molecular reactions unfortunately prevents a quantitative discussion on the possible effects of non-equilibrium chemistry.

Key words. Convection – Line: formation – Stars: abundances – Stars: atmospheres – Stars: Population II – Galaxy: evolution

1. Introduction

Oxygen is the third most abundant element in the Universe after hydrogen and helium. Besides being relatively common, oxygen has also attracted a great deal of attention due to its special role in galactic and stellar evolution. Since oxygen is predominantly produced in connection with core collapses of massive stars (type II supernovae, SNe II) while iron is also forged during accretion-induced collapses of white dwarfs (type Ia supernovae, SNe Ia), the abundance ratio of these two elements at different cosmic epochs give important insight to the formation and evolution of the Galaxy, as well as constraining the physics of supernovae. The amount of oxygen in stars can also significantly influence the nuclear energy production and the opacities, which affects stellar evolution. As a consequence, the dating of globular clusters depend on the stellar oxygen content: an increase of the oxygen over-abundance [O/Fe][1] from +0.3 to +1.0 introduces an about 2 Gyr lower age of the oldest clusters (VandenBerg & Bell 2001). Additionally, the light

elements Li, Be and B are produced through cosmic ray spallation of C, N and, most importantly, O with protons and α-particles. Thus, a proper understanding of the oxygen abundances of stars of different metallicities is required in order to interpret the evolution of the light elements.

Following the first indication of an oxygen over-abundance relative to iron ([O/Fe] > 0) in metal-poor stars (Conti et al. 1967), a great number of studies have been devoted to quantify this enhancement. Although all agree on its existence, the amount of the over-abundance is hotly contested. Various oxygen diagnostics in different types of stars have been applied but with disparate results. The forbidden [O I] lines at 630.0 and 636.3 nm in metal-poor giants suggest a nearly flat plateau at [O/Fe] ~ 0.4 for [Fe/H] $\lesssim -1.0$ (e.g. Barbuy 1988; Sneden et al. 1991) while the O I triplet at 777 nm in metal-poor dwarfs and subgiants tend to imply systematically higher values, often with a monotonic increase towards lower metallicities (e.g. Abia & Rebolo 1989; Israelian et al. 1998, 2001; Boesgaard et al. 1999; Carretta et al. 2000).

All oxygen criteria have their pros and cons, which influence the conclusions. The forbidden lines are immune to departures from local thermodynamic equilibrium (LTE) (cf. dis-

---

Send offprint requests to: e-mail: martin@astro.uu.se

[1] The abundance ratios are defined by the customary [X/Fe]=$\log(N_{\rm X}/N_{\rm Fe})_* - \log(N_{\rm X}/N_{\rm Fe})_\odot$

cussion in Kiselman 2001) but the lines are very weak at low metallicities, in particular in unevolved stars where the feature becomes undetectable for [Fe/H] $\lesssim -2.0$ (Nissen et al. 2001). Furthermore, concerns regarding the primordial nature of the oxygen in field giants have been voiced as mixing of nuclear-processed material may pollute the surface, as evident in many globular cluster giants (e.g. Langer et al. 1997). The O I triplet on the other hand is more easily discerned in metal-poor dwarfs but also more susceptible to departures from LTE (cf. Kiselman 2001 and references therein) and inhomogeneities introduced by stellar granulation (Kiselman & Nordlund 1995) than the [O I] lines. The high excitation potential of the O I lines also make them vulnerable to errors in the effective temperature ($T_{\rm eff}$). Additionally, an often overlooked source of confusion is the stellar Fe abundances, which should be self-consistently computed in order to obtain reliable [O/Fe] ratios. Finally, even the question of the absolute solar oxygen abundance is still not settled, leaving the fundamental reference point for stellar [O/Fe] ratios insecurely anchored.

An attractive alternative to the O I and [O I] lines are provided by the molecular OH electronic transitions in the UV. (Bessell et al. 1984, 1991; Nissen et al. 1994). In fact, at [Fe/H] ~ -4 no substitute for the OH lines as the prime oxygen diagnostic is available. Therefore the OH spectral line formation must be properly understood when attempting to probe the earliest epochs of the Galactic evolution for example to identify the nucleosynthetic fingerprints of the elusive Population III stars (e.g. Karlsson & Gustafsson 2001). Recently, Israelian et al. (1998, 2001) and Boesgaard et al. (1999) have analysed the UV OH ($A^2\Sigma$ - $X^2\Pi$) lines in stars down to [Fe/H] $\simeq -3.3$ with high S/N and resolution spectra and have found a linear trend in [O/Fe] vs [Fe/H] with a slope of about -0.4^2, in stark conflict with the [O I] results. If confirmed, these results would have far-reaching consequences, as outlined above. The situation is complicated, however, by recent studies of the OH vibrational-rotational lines in the infrared (IR), which suggest a nearly flat [O/Fe] in agreement with the [O I] findings (Balachandran et al. 2001; Melendez et al. 2001).

As all previous investigations have been based on 1D hydrostatic model atmospheres, one may worry about possible systematic errors introduced by the inherent assumptions of the analyses. Recently the first 3D hydrodynamical model atmospheres of metal-poor stars have been constructed (Asplund et al. 1999a), which have very different temperature structures compared with classical 1D model atmospheres. As a consequence, analyses of temperature sensitive spectral features can be suspected to be systematically in error if relying on 1D model atmospheres. In particular, Asplund et al. (1999a) cautioned that oxygen abundances of metal-poor stars derived from 1D studies of OH lines may be strongly overestimated due to the extreme temperature sensitivity of molecule formation. The aim of the present paper is to quantify this suspicion in terms of O abundances and investigate other possible systematic errors which may hamper the 3D analysis of OH lines. Preliminary results have been presented in Asplund (2001).

2. 3D hydrodynamical model atmospheres

Realistic *ab-initio* 3D, time-dependent simulations of stellar surface convection form the foundation for the present study. The same incompressible radiative hydrodynamical code which previously has been applied successfully to studies of solar (e.g. Stein & Nordlund 1998; Asplund et al. 2000a,b) and stellar granulation (e.g. Asplund et al. 1999a, Allende Prieto et al. 2001; Asplund et al., in preparation) has here been used to construct sequences of 3D model atmospheres with varying stellar parameters. The equations of mass, momentum and energy conservation together with the simultaneous treatment of the 3D radiative transfer equation have been solved on a Eulerian mesh with 100 x 100 x 82 gridpoints. The physical dimensions of the numerical grid were sufficiently large to cover many ($\gtrsim 10$) granules simultaneously. The depth scales have been optimized to provide the best resolution where it is most needed, i.e. in those layers with the steepest gradients in terms of dT/dz and d^2T/dz^2, which for the solar-type stars occurs around the visible surface.

Special care has been exercised to include the most appropriate input physics. In particular, state-of-the-art equation-of-state (Mihalas et al. 1988), which includes the effects of ionization, excitation and dissociation of the most important atoms and molecules, and relevant continuous (Gustafsson et al. 1975 with subsequent updates) and line (Kurucz 1993) opacities have been employed. During the convection simulations, the 3D radiative transfer is solved for in total eight inclined rays under the simplifying assumptions of LTE ($S_\nu = B_\nu$) and grouping of the opacities into four bins (Nordlund 1982). At regular intervals during the simulations, the accuracy of the opacity binning technique is verified by solving the full monochromatic radiative transfer (about 2700 wavelength points) in the 1.5D approximation, i.e. treating each vertical column as a separate 1D model atmosphere and ignoring all horizontal radiative transfer effects. Further details on the numerical procedures of the simulations may be found in Stein & Nordlund (1998).

For the present purpose, two sequences of 3D model atmospheres have been constructed. The first series of models (here: the solar sequence) correspond to the Sun ($T_{\rm eff} \simeq 5800\,{\rm K}\,^3$, $\log g = 4.44$ [cgs]) but with a range of metallicities

---

[2] When restricting to the OH-based results and taking the errors in both [Fe/H] and [O/Fe] into account, the Boesgaard et al. (1999) data gives a slope of -0.40 ± 0.04 and -0.36 ± 0.04 for the King (1993) and Carney (1983) $T_{\rm eff}$-scales, respectively. Similarly, the published results of Israelian et al. (1998) are consistent with a slope of -0.38 ± 0.07, which becomes -0.37 ± 0.06 when also including the new OH data in Israelian et al. (2001). For simplicity we here adopt a slope of -0.40 but emphasize that the exact value only has a marginal effect on our results. It should be noted that the values given in the original references are slightly smaller due to the combination of OH and O I results (Boesgaard et al.) and restriction to stars with [Fe/H] ≤ -1.0 (Israelian et al.). When also considering the non-LTE results for Fe I by Thevenin & Idiart (1999), the slopes decrease by about 0.06 (King 2000; Israelian et al. 2001), but cf. discussion in Sect. 5.4.

[3] Since the entropy of the inflowing gas at the lower boundary has replaced $T_{\rm eff}$ as an independent input parameter in 3D convection simulations, the resulting $T_{\rm eff}$ varies slightly in time due to the evolution of individual granules. In order to obtain a specific temporally aver-

Table 1. Details of the 3D hydrodynamical model atmospheres

$< T_{\mathrm{eff}} >$ [a] [K]	$\log g$ [cgs]	[Fe/H]	x,y,z-dimensions [Mm]	time[b] [min]
5767 ± 21	4.44	$+0.0$	$6.0 \times 6.0 \times 3.7$	50
5822 ± 11	4.44	-1.0	$6.0 \times 6.0 \times 3.7$	50
5837 ± 8	4.44	-2.0	$6.0 \times 6.0 \times 3.7$	40
5890 ± 8	4.44	-3.0	$6.0 \times 6.0 \times 3.7$	40
6191 ± 37	4.04	$+0.0$	$21.4 \times 21.4 \times 8.7$	60
6180 ± 20	4.04	-1.0	$21.4 \times 21.4 \times 8.7$	60
6178 ± 17	4.04	-2.0	$21.4 \times 21.4 \times 8.7$	60
6205 ± 15	4.04	-3.0	$21.4 \times 21.4 \times 8.7$	60

[a] The temporal average and standard deviation of the emergent T_{eff} of the different convection simulations

[b] The time coverage of the part of the simulation used for the spectral line calculations, while the full convection simulations are much longer extending over several convective turn-over time-scales

([Fe/H] = 0.0, -1.0, -2.0 and -3.0), while the second suite (here: the turn-off sequence) correspond to typical turn-off stars ($T_{\mathrm{eff}} \simeq 6200$ K, $\log g = 4.04$ [cgs]), again with varying metal content ([Fe/H] = 0.0, -1.0, -2.0 and -3.0). Some details of the simulations are given in Table 1. The individual elemental abundances have been taken from Grevesse & Sauval (1998) scaled appropriately to the relevant [Fe/H] with no α-element enhancements. As long as the comparison is strictly differential between the 3D and 1D model atmospheres as in our case the omission of α-element enhancements will be negligible for the spectral line formation. The initial snapshots for the simulations were taken from simulations of lower numerical resolution ($50 \times 50 \times 82$), which had been run sufficiently long times to allow thermal relaxation and a statistically steady state at the wanted T_{eff} to be established. The initial snapshots for these lower resolution runs in turn were obtained from a previous solar simulation (Stein & Nordlund 1998) scaled appropriately to the new stellar parameters using the experience from 1D hydrostatic stellar models and the entropy variations in 2D hydrodynamical model atmospheres (Ludwig et al. 1999; Freytag et al. 1999). Classical 1D, hydrostatic MARCS model atmospheres (Asplund et al. 1997) with identical input parameters and chemical compositions as the 3D simulations have been constructed to allow a differential comparison in terms of spectral line formation. Whether 3D models indeed should be assigned the same T_{eff} as a corresponding 1D model atmosphere is investigated in Sect. 5.2 when comparing the predictions for the infrared flux method (IRFM) with the two types of models.

aged value for the emergent T_{eff}, a careful and very time-consuming fine-tuning of the inflowing entropy would be required. Since we are only interested in a differential comparison between 3D and 1D, we have not attempted to obtain exactly the solar T_{eff} for the individual simulations and instead settled for values in reasonable proximity of the targeted T_{eff}, cf. Table 1. Naturally, the comparison 1D model atmospheres have the same T_{eff} as the final 3D average to isolate the granulation effects from differences in input parameters.

Although the details of the convection properties of the present and other simulations for late-type stars will be described elsewhere (Asplund et al., in preparation), the most important metallicity effects on the resulting photospheric structures are briefly discussed here in order to understand the impact of the 3D models on the spectral line formation of the OH lines. While the temperature remains close to the radiative equilibrium value at solar metallicities and mild metal-deficiencies ([Fe/H]$\gtrsim -1.0$), the temperature in the outer layers depart significantly from it at lower metallicities (Asplund et al. 1999a). The temperature in this optically thin region is determined from a competition between adiabatic cooling and radiative heating. The latter mechanism arises when continuum photons released at deeper layers are reabsorbed in spectral lines. At solar metallicities the abundant spectral lines succeed in providing sufficient radiative heating to balance the adiabatic cooling and keeping the average temperature close to the radiative equilibrium expectation. At progressively lower metallicities, the available spectral lines become fewer and weaker, which allows cooling to dominate more. As a consequence, balance is not restored unless the temperature is much below the radiative equilibrium value. Thus, in hydrodynamical model atmospheres spectral lines have the opposite effect compared to in hydrostatic model atmospheres which enforce radiative equilibrium: *spectral lines cause surface heating*. The effects of the lower temperatures are first visible at the outermost layers but move towards deeper layers at progressively lower metallicities.

When viewed as a function of optical depth instead of geometrical height, the low surface temperatures are less pronounced since the temperature sensitivity of the continuous opacities partly hides the effect (Asplund et al. 1999a); lower temperatures also imply smaller opacities and optical depths. Nevertheless the low temperatures reach typical line-forming regions at low metallicities. Furthermore, the cool outer layers shift the whole line formation outwards for temperature sensitive features such as molecular lines. For example, at $\log \tau_{500} = -3$ the average temperature difference between 3D and 1D models can reach 1000 K and thus have a profound effect on the lines sensitive to those layers.

Differences in the gas and electron pressures could also influence spectral line formation. With the exception of some additional contribution from turbulent pressure in the convective overshoot region around the visual surface, the total pressure is well approximated by the gas pressure in the photosphere for late-type dwarfs. Since even in the 3D hydrodynamical models the photosphere is typically not too far from hydrostatic equilibrium, the pressure scale height $H_{\mathrm{P}} = -(\mathrm{d}\ln P/\mathrm{d}r)^{-1} \approx P_{\mathrm{gas}}/g\rho \propto T$ and thus the resulting 3D pressure structure tend to be lower than the corresponding 1D value at a given geometric height at low metallicities. Naturally, the lower temperatures have an even greater impact on the electron pressure. The lower gas and electron pressures in metal-poor 3D model atmospheres will affect mainly lines that are considered gravity sensitive.

3. Spectral line formation in 3D model atmospheres

The OH line calculations with the 3D hydrodynamical model atmospheres follow the same procedure as in other recent investigations of the influence of granulation on stellar spectroscopy (Asplund et al. 1999a,b, 2000a,b,c; Asplund 2000a,b, 2001; Asplund & Carlsson 2001; Allende Prieto et al. 2001; Nissen et al. 2000, 2001; Primas et al. 2000). The 3D convection simulations, which extend down to the essentially adiabatic layers well below the visible photosphere, were interpolated to a finer vertical depth-scale although with the same number of depth-points to improve the numerical accuracy in the spectral synthesis. The average continuum optical depth range typically beyond $\log \tau_{500} \gtrsim 2$ and above $\log \tau_{500} \lesssim -5$, in order to minimize the influence from the artificial top and bottom boundaries. Prior to the line transfer calculations the horizontal resolution was decreased from $100 \times 100 \times 82$ to $50 \times 50 \times 82$ to ease the computational burden; various tests ensured that the procedure did not introduce any differences in the spatially and temporally averaged line profiles. From the full convection simulations, which cover several convective turn-over time-scales, representative sequences of typically one hour stellar time with snapshots every 30 s were selected for the spectral syntheses. In terms of derived oxygen abundances, the number of snapshots were sufficient to provide statistically significant results ($\Delta \log \epsilon_O < 0.01$ dex), as verified by test calculations with shorter time sequences. The mean T_{eff}'s for the shorter simulation sequences are given in Table 1.

The spectral line formation in 3D model atmospheres was performed under the assumption of LTE. Thus, the OH number densities were computed from instantaneous molecular equilibrium and Saha ionization and Boltzmann excitation balances. The line source function was approximated with the Planck function ($S_\nu = B_\nu$). The applicability of these strong assumptions is further investigated in Sects. 5.5 and 5.6. The OH molecular equilibrium was computed with scaled solar abundances with the exception of the oxygen abundance. The removal of available oxygen atoms due to CO formation was taken into account but the effect was found to be negligible. Flux profiles were computed for two typical OH UV lines (313.9 and 316.7 nm) from solving the radiative transfer for in total 17 inclined rays (four μ-angles and four φ-angles plus the vertical $\mu = 1.0$). The line transition data for the OH lines was taken from Israelian et al. (1998); we emphasize that in a differential 3D-1D comparison such as ours the exact choices of for example the gf-values are not important. In addition, we have included six of the Fe II lines used by Nissen et al. (2001) in their study of [O/Fe] from the [O I] line to quantify the corresponding impact on Fe abundances. The background continuous opacities were calculated using the Uppsala opacity package (Gustafsson et al. 1975 with subsequent updates). Since the Doppler shifts introduced by the convective velocity field are fully accounted for, no microturbulence or macroturbulence parameters enter the 3D line calculations (Asplund et al. 2000b,c). It is noteworthy that none of the various free parameters hampering 1D analyses (e.g. mixing length parameters, micro- and macroturbulence) are necessary with 3D hydrodynamical model atmospheres. For the 1D calculations, a microturbulence of $1.0 \, \text{km s}^{-1}$ has been assumed for the solar and turn-off sequences; the choice of microturbulence, however, is only of some significance for the solar metallicity models while unimportant at low metallicities.

The main advantage of limiting the comparison to a strictly differential study of the 3D and 1D predictions is that the uncertainties in e.g. the absolute transition probabilities, equivalent widths, blends, continuum placement, missing UV opacities, T_{eff}-calibration and the solar oxygen abundance can be avoided. As a consequence we are not able to determine accurate *absolute* stellar oxygen abundances. Instead we only attempt to address the question of whether there are systematic errors in analyses of the UV OH lines when relying on classical 1D model atmospheres. A star-by-star analysis of high quality OH observations is left for a future paper.

4. 3D LTE oxygen abundances derived from UV OH lines

Molecule formation is extremely temperature sensitive (as long as the molecule in question is a trace element for its atomic constituents, which is the case for OH in the stars studied here). For conditions typical of the line-forming regions in the Sun, the LTE number density of OH, N_{OH}, is proportional to $\approx T^{-12}$ as estimated from our adopted equation-of-state and molecular balance routines. This high degree of non-linearity makes molecular lines very susceptible to errors in the adopted temperature structures of the model atmospheres. In particular, the very different temperature structures of typical convective up- and downflows compared with classical 1D model atmospheres (i.e. up- and downflows can *not* be represented by two theoretical hydrostatic model atmospheres with different T_{eff}, since granules have a much steeper temperature gradient than intergranular lanes), can be suspected to significantly influence the molecular number densities and line formation.

Under the assumption of LTE adopted here, N_{OH} depend only on the instantaneous local temperature. In general the temperature contrast reverses in the convective overshoot region some distance above the continuum forming layers, i.e. gas above the warm, upflowing granules tend to be *cooler* than average (e.g. Stein & Nordlund 1998). In particular in metal-poor stars the horizontal temperature contrast is very large due to the weak coupling between the gas and the radiation field (Asplund et al., in preparation). In general the temperatures at the high atmospheric layers are very low but occasionally the compression from converging gas flows or shocks can rise the temperature to the radiative equilibrium value or even above it. As a consequence, the UV OH LTE line strengths across the stellar granulation are expected to be stronger in the granules but with pronounced scatter when viewed nearly face-on, as confirmed by the 3D line calculations (Fig. 1). The spatially and temporally averaged OH flux profiles are therefore strongly biased towards upflowing regions due to their higher contin-
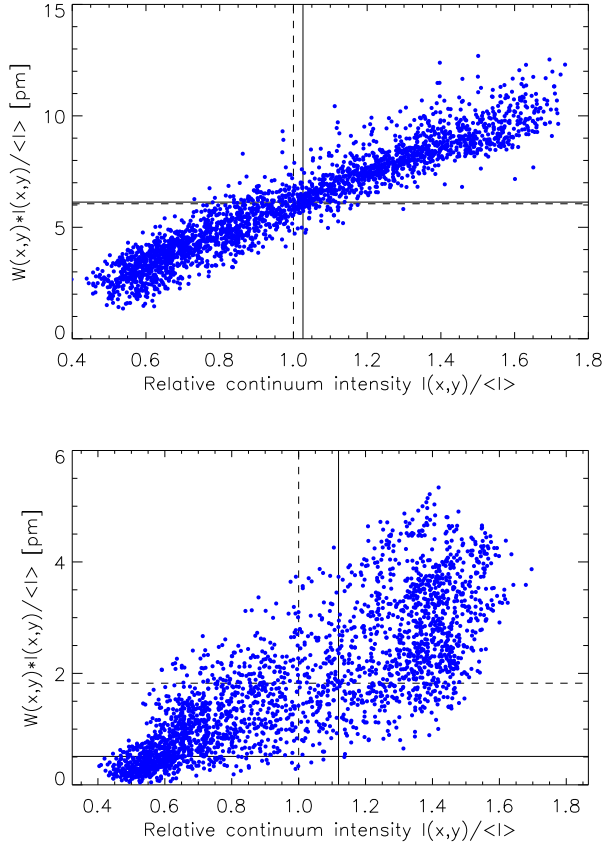
Fig. 1. The contribution to the equivalent width, $W_\lambda(x, y) \cdot I_\lambda^{cont}(x, y)/\langle I^{cont}\rangle$, of the OH 313.9 nm line across the stellar surface for the [Fe/H]= +0.0 (*Upper panel*) and [Fe/H]= −3.0 (*Lower panel*) models in the solar sequence as a function of the relative continuum intensity $I_\lambda^{cont}(x, y)/\langle I^{cont}\rangle$ at 313.9 nm. The spatially resolved intensity profiles have been computed for $\mu = 1.0$. The horizontal and vertical dashed lines denote the mean equivalent widths and continuum intensities with 3D model atmospheres, while the solid lines mark the corresponding 1D predictions using the same O abundances as in 3D. Note that the here shown 3D calculations only refer to one snapshot each for the two models and not the whole simulation sequences

uum intensities, steeper temperature gradients and larger area coverage [4].

Typical resulting 3D and 1D line profiles are shown in Fig. 2, which clearly illustrates the influence of 3D models on the derived O abundances from UV OH lines at low metallicities. The much lower temperatures and larger concentration of OH molecules in the 3D model atmospheres of metal-poor stars result in far stronger OH lines than with 1D model atmospheres while the difference is much less accentuated at solar metallici-

---

[4] Note that the opposite is true for the OH pure rotational lines in the IR since these lines and their surrounding continuum are formed at significantly higher layers where the temperature contrast is reversed relative to the visual continuum (cf. Figs. 1 and 7 in Kiselman & Nordlund 1995)
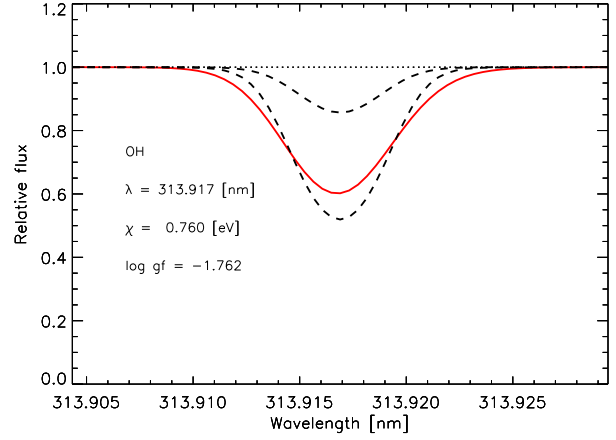

Fig. 2. The predicted profile for the OH 313.9 nm line using the 3D hydrodynamical model atmosphere for Teff=5800 K, logg=4.44 [cgs], [Fe/H]=-3.0 with an adopted O abundance of $\log \epsilon_O = 6.4$ (solid line). In comparison the corresponding 1D profile with the same abundance is much weaker (upper dashed line). Only with $\log \epsilon_O = 7.05$ (lower dashed line) is the 1D profile comparable in strength to the 3D profile. In no cases have extra broadening in the form of rotation or macroturbulence been applied

Table 2. Comparison of the oxygen LTE abundances derived with 1D hydrostatic and 3D hydrodynamical model atmospheres. The 3D O abundances are those which reproduce the equivalent widths computed using a 1D model atmosphere, a microturbulence of $\xi_{turb} = 1.0$ km s^{-1} and the oxygen abundances given in the fourth column

T_{eff} [K]	$\log g$ [cgs]	[Fe/H]	$\log \epsilon_{O,1D}$	$\log \epsilon_{O,3D}$ 313.9 nm[a]	$\log \epsilon_{O,3D}$ 316.7 nm[b]
5767	4.44	+0.0	8.90	8.88	8.89
5822	4.44	−1.0	8.30	8.03	8.07
5837	4.44	−2.0	7.70	7.19	7.25
5890	4.44	−3.0	7.10	6.44	6.52
6191	4.04	+0.0	8.90	8.80	8.82
6180	4.04	−1.0	8.30	7.97	8.00
6178	4.04	−2.0	7.70	6.90	7.01
6205	4.04	−3.0	7.10	6.08	6.22
HM, int.[c]	4.44	+0.0	8.90	8.69	8.72
HM, flux[c]	4.44	+0.0	8.90	8.64	8.69

[a] $\log gf = -1.76$, $\chi_{exc} = 0.76$ eV (Israelian et al. 1998)
[b] $\log gf = -1.69$, $\chi_{exc} = 1.11$ eV (Israelian et al. 1998)
[c] Using the Holweger-Müller (1974) 1D semi-empirical model atmosphere for the solar case instead of a MARCS solar model, either using intensity or flux line profiles

ties, in accordance with the behaviour of the temperature structures. Table 2 lists the O abundances of the two OH lines for the two types of model atmospheres. The 3D O abundances are those which reproduce the equivalent widths computed using 1D model atmospheres and an adopted [O/Fe] = −0.40·[Fe/H] trend (Israelian et al. 1998, 2001; Boesgaard et al. 1999). A

less steep [O/Fe] trend would have resulted in slightly smaller granulation effects due to the shifting of the line-formation region inwards where the low temperatures in the 3D models are less pronounced. Similarly, the impact of the 3D models is greater for the OH 313.9 nm line than for the OH 316.7 nm line in accordance with the lower excitation potential and larger line strength of the former. The in general larger granulation corrections for the hotter models are in agreement with their larger temperature differences and the high non-linearity of the OH line formation.

For completeness we have carried out an identical 3D-1D comparison for six Fe II lines. The resulting granulation corrections are listed in Table 3. As expected (Asplund et al. 1999a), the impact of 3D model atmospheres are relatively minor on the Fe II lines since they are formed in deep atmospheric layers and therefore not sensitive to the low temperatures encountered in the upper layers in the 3D models. In terms of Fe abundance, the difference between the 1D and 3D predictions amounts to $\lesssim 0.1$ dex.

The strong metallicity dependence of the abundance corrections has a profound impact on the use of UV OH lines as O diagnostic in metal-poor stars and cast serious doubts on recent claimed linear trends in [O/Fe] towards lower metallicities based on 1D LTE analyses (Israelian et al. 1998, 2001; Boesgaard et al. 1999). In Fig. 3 the average granulation corrections of the two investigated OH lines for the solar and turn-off sequences are shown, while Fig. 4 presents the final mean corrections of the different T_{eff} simulations [5]. The correction of the 1D LTE result due to the use of 3D model atmospheres is here defined as relative to the solar calibration, i.e. the abundance differences in Table 2 are subtracted with the corresponding effect for the Sun since [O/Fe] ratios are studied. This procedure is similar to the common practice of determining astrophysical gf-values from the Sun, as was also the basis for the works by Nissen et al. (1994), Israelian et al. (1998, 2001) and Boesgaard et al. (1999). For the Sun, two possible calibrations are possible using either the Holweger-Müller (1974) semi-empirical model atmosphere or the theoretical MARCS model as the 1D representation of the solar photosphere, yielding two possible 3D trends in Figs. 3 and 4. The difference between the two trends therefore simply reflects the difference in derived solar O abundances when relying on the two types of 1D model atmospheres. It should be noted that the granulation corrections for Fe II lines presented in Table 3 are *not* included in Figs. 3 and 4, since the adopted [O/Fe] trend with metallicity originates from analyses of Fe I lines (Boesgaard et al. 1999; Israelian et al. 1998, 2001, cf. discussion in Sect. 5.4). According to Table 3, the inclusion of the Fe II results would bring down the 3D LTE [O/Fe] results further by $\lesssim 0.1$ dex at the lowest metallicities.

Taken at face value, with the claimed 1D [O/Fe] results and the here presented granulation corrections, the emerging trend with metallicity is in fact roughly consistent with the since long advocated [O/Fe] plateau from [O I] lines, as seen in Fig. 4. However, we caution that such a conclusion is likely premature.

---

[5] The results shown in Fig. 4 differ slightly from those presented in Asplund (2001) due to the inclusion of additional lines and simulations and use of more temporally extended 3D model atmospheres.
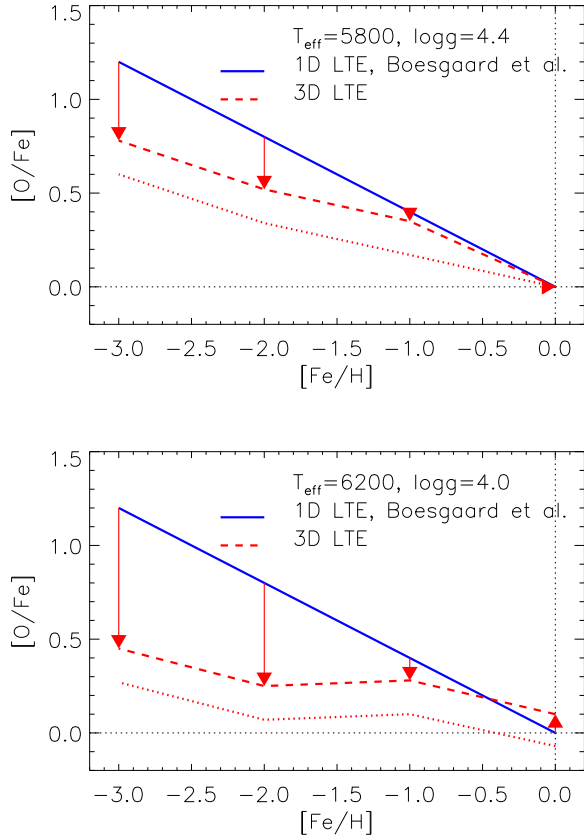
Table 3. Comparison of the iron LTE abundances derived with 1D hydrostatic and 3D hydrodynamical model atmospheres from Fe II lines. The 3D Fe abundances are those which reproduce the equivalent widths computed using a 1D model atmosphere, a microturbulence of $\xi_{\mathrm{turb}} = 1.0\,\mathrm{km\,s^{-1}}$ and the Fe abundances given in the fourth column

T_{eff} [K]	$\log g$ [cgs]	[Fe/H]	$\log \epsilon_{\mathrm{Fe,1D}}^{\mathrm{a}}$	$\log \epsilon_{\mathrm{Fe,3D}}^{\mathrm{a}}$	$\Delta\log\epsilon_{\mathrm{Fe}}$
5767	4.44	+0.0	7.50	7.48	−0.02
5822	4.44	−1.0	6.50	6.54	+0.04
5837	4.44	−2.0	5.50	5.60	+0.10
5890	4.44	−3.0	4.50	4.59	+0.09
6191	4.04	+0.0	7.50	7.49	−0.01
6180	4.04	−1.0	6.50	6.52	+0.02
6178	4.04	−2.0	5.50	5.56	+0.06
6205	4.04	−3.0	4.50	4.57	+0.07
HM, int.[b]	4.44	+0.0	7.50	7.52	+0.02
HM, flux[b]	4.44	+0.0	7.50	7.48	−0.02

[a] The impact of 3D model atmospheres on the derived stellar metallicities have been investigated for in total six Fe II lines (614.9, 623.8, 624.7, 641.7, 643.2 and 645.6 nm). In all cases the different Fe II lines give the same granulation corrections to within 0.03 dex.

[b] Using the Holweger-Müller (1974) 1D semi-empirical model atmosphere for the solar case instead of a MARCS solar model, either using intensity or flux line profiles

ture, as there still exist inherent assumptions and approximations in the present 3D analysis, most notably the use of instantaneous molecular equilibrium and LTE radiative transfer (Sects. 5.5 and 5.6), besides of course the fact that no direct comparison with observations on a star-by-star basis has been made. Furthermore, the issues of possible missing UV opacities (Balachandran & Bell 1998; Bell et al. 2001) and stellar Fe abundances (Thevenin & Idiart 1999; King 2000, cf. Sect. 5.4) must be addressed before safe conclusions can be drawn from OH lines regarding the [O/Fe] behaviour in metal-poor stars. Therefore, we here refrain from claiming accordance between the UV OH and [O I] results and instead settle to point out a possible serious systematic error affecting recent 1D analyses of OH lines. As a result, the case for a continuous linear increase in [O/Fe] towards lower metallicities is seemingly much weakened.

Naïvely, one could expect that all OH molecular lines should be similarly affected by the low temperatures and high molecular number densities in the 3D model atmospheres of metal-poor stars. In view of this, the low [O/Fe] values found from OH vibrational-rotational lines in the IR from cool ($T_{\mathrm{eff}} \lesssim 5000\,\mathrm{K}$) metal-poor giants and dwarfs (Balachandran et al. 2001; Melendez et al. 2001) appear surprising. No 3D hydrodynamical model atmospheres are yet available for these lower T_{eff} and/or surface gravities while the IR lines are unpropitiously weak for the stellar parameters of the current ($T_{\mathrm{eff}} \gtrsim 5800\,\mathrm{K}$) suites of models. Hence we are unable to confirm or disprove this apparent discordance. However, we have verified that OH lines in the IR with similar line strengths as
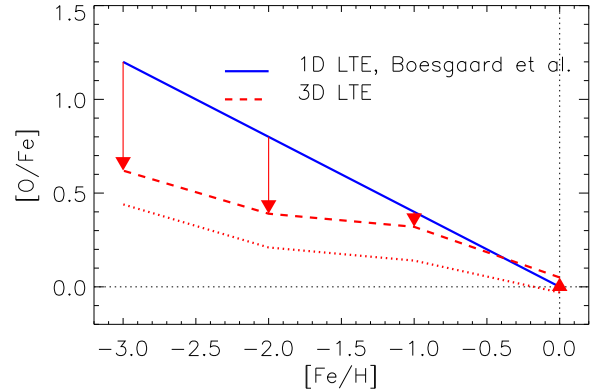
Fig. 4. The impact of the 3D LTE analysis of the OH lines on the [O/Fe] trend in metal-poor stars when averaging the granulation corrections for the solar and turn-off sequences for the two OH lines 313.9 and 316.7 nm. As in Fig. 3, both the cases when using the Holweger-Müller (1974) model atmosphere (dashed line) and the MARCS model atmosphere (dotted line) for the solar calibration are shown. It should be emphasized that the assumption of LTE in the molecule formation and radiative transfer may skew the results according to the discussion in Sect. 5

Fig. 3. The impact of 3D model atmospheres on the [O/Fe] trend with metallicity for the solar (*Upper panel*) and turn-off (*Lower panel*) sequences. The solid line represents the 1D LTE result of Boesgaard et al. (1999) based on only the UV OH lines and the King (1993) $T_{\rm eff}$-scale: [O/Fe] = $-0.40\cdot$[Fe/H]. The dashed and dotted lines denote the typical O abundance corrections in a 3D LTE analysis (average for the OH 313.9 and 316.7 nm lines) compared with the 1D case depending on the choice for the solar calibration. For the former the Holweger-Müller (1974) semi-empirical solar atmosphere with intensity profiles has been used while for the latter a theoretical MARCS model atmosphere together with flux profiles have been adopted; for all other 1D models theoretical MARCS models have been utilised. Hence, in the upper panel the granulation correction for the [Fe/H]=0.0 model is forced to disappear since it corresponds to the Sun

the UV lines suffer from as severe granulation abundance corrections for the models listed in Table 1 using fake OH lines with strongly enhanced transition probabilities. Thus, the spectral locations of the transitions are not a solution to this conundrum. Whether the differences in stellar parameters may be a possible resolution is discussed further in Sect. 6.

5. Possible systematic errors affecting the 3D results

5.1. Temperature structure in 3D model atmospheres

The large granulation effects on the derived O abundances for OH lines in metal-poor stars hinge crucially on the existence of the low atmospheric temperatures encountered in the OH line-forming region with 3D model atmospheres. It is therefore natural to inquire whether the resulting temperature structures are indeed accurate representations of the real stellar atmospheres. Even if the here employed 3D hydrodynamical model atmospheres no longer rely on the same simplifying assumptions as in classical 1D model atmospheres, uncertainties in the temperature structures may still remain. A consistency check on the 3D atmospheres is available from similar 2D radiative-hydrodynamical simulations (Ludwig et al. 1999; Freytag et al. 1999), which also produce the distinct sub-radiative equilibrium temperatures. This consonance is reassuring but not too surprising given the resemblance in the underlying assumptions of the two types of simulations.

As explained in Sect. 4, the low atmospheric temperatures are natural consequences of no longer enforcing radiative equilibrium and instead solving explicitly the time-dependent energy equation. This phenomenon is therefore a real physical effect which must be present in the photospheres of metal-poor stars. Nevertheless, the magnitude of the effect may have been overestimated in the present simulations. Asplund et al. (1999a) indeed cautioned that the neglect of Doppler shifts in the treatment of the strong spectral lines in the construction of the 3D model atmospheres may lead to the radiative heating being underestimated. Work is currently being undertaken to construct such further improved 3D model atmospheres.

An alternative avenue to proceed is to design observational tests to confront the predictions from 3D model atmospheres with. An often-used method is a detailed comparison of spectral line asymmetries and shifts (e.g. Asplund et al. 2000a,b; Allende Prieto et al. 2001). Unfortunately, a similar study of the asymmetries of the OH lines is unlikely to give crucial clues due to the inevitable blends in the UV. Furthermore, only limited guidance is likely to be obtained from studies of line asymmetries of atomic species since they do not probe the same high atmospheric layers as the molecular transitions.

A possible venture to explore is the individual O abundances obtained from a large sample of OH lines of different excitation potential. Since the exact 3D abundance corrections depend on the transition properties with low-excitation and strong lines being more influenced by the 3D model atmospheres (Table 2), different results are expected compared with 1D model atmospheres. An examination of Table 3 in Israelian et al. (1998) indeed reveals that low excitation OH lines (e.g. 312.39, 312.81, 312.83 nm, $\chi_{exc} \simeq 0.2$ eV) appear to systematically give $\simeq 0.1$ dex higher abundance than the high excitation lines (e.g. 316.71, 320.39, 325.55 nm, $\chi_{exc} \simeq 0.8 - 1.3$ eV) in a 1D analysis, hinting to a possible problem in the 1D temperature structures at low metallicities *relative to the Sun*. However there is no clear trend with metallicity in the differences in the derived O abundances but the scatter is unfortunately very large. A proper investigation will therefore require many more lines for a larger stellar sample. Furthermore, a prerequisite is an accurate determination of the stellar parameters, which, in view of the current disagreement on the T_{eff}-scale of metal-poor stars, is unlikely to be settled for good in the near future.

5.2. Effective temperature

In order to obtain accurate absolute abundances, not only a realistic model of the stellar photosphere and a proper understanding of the line formation process are necessary but also appropriate fundamental stellar parameters. For OH lines, the effective temperature is of special importance. In Sect. 4 the comparison between the 3D and 1D predictions were carried out assuming that the relevant T_{eff} should be the same for the two types of models.

One may suspect that the presence of temperature inhomogeneities in the continuum-forming layers should make the emergent flux distribution different in 3D model atmospheres compared with homogeneous 1D models, in particular for metal-poor stars which often are characterized by "naked granulation" (Nordlund & Dravins 1990; Asplund et al., in preparation): the region of maximum horizontal temperature contrast reaches the visible surface whereas for example for the Sun these layes are hidden slightly below the photosphere (Stein & Nordlund 1998). This difference will be particularly manifested in UV colours (amounting to $\lesssim 10\%$ in continuum fluxes at 314 nm, cf. Fig. 1) while the effect is minimized at IR wavelengths. Since IRFM is our preferred choice for T_{eff}-calibrations, we will here only investigate the impact of 3D models on this method.

The IRFM is designed to compare the observed ratio of the total bolometric flux of a star and a monochromatic continuum flux at IR wavelengths with the corresponding theoretical ratio from model atmospheres (Blackwell & Shallis 1977), In practice, JHK photometry normally replaces the monochromatic continuum flux for observational convenience. Here we follow the original idea by computing the spatially and temporally averaged continuum flux at $2.2\,\mu$m for the various 3D simulations and compare these predictions with corresponding ones for 1D model atmospheres with $T_{eff,3D}$ and $T_{eff,3D} \pm 100$ K to quantify typical corrections to T_{eff}-estimates based on the IRFM and classical 1D model atmospheres. It should be noted that our procedure thus neglects the model atmosphere dependence in estimating the stellar fluxes *outside* the observed photometric bands to obtain bolometric fluxes (Alonso et al. 1995). However, only a small fraction ($\lesssim 10\%$) of the total flux is carried at those wavelengths for the F-K stars of interest here and the slight inconsistency of relying on 1D models for this purpose should have a marginal effect on the final T_{eff}-calibration.

The differences in T_{eff}-determinations from 3D and 1D model atmospheres are shown in Fig. 5. Clearly due to the small model sensitivity of the method, the use of 1D models in available IRFM determinations does not significantly encumber the results. For the solar sequence the T_{eff} differences amount to typically 20 K while the modifications for the turn-off sequence are completely negligible. The smaller effect for the hotter models is in accordance with the relatively smaller fraction of the total flux emitted at IR wavelengths and thus smaller sensitivity of the temperature structure of the adopted model atmospheres. In view of the typical observational uncertainties of ≈ 100 K currently attached to IRFM, the errors in IRFM T_{eff} estimates are still very much dominated by the accuracy of the observations rather than the adopted model atmospheres.

The small influence on T_{eff} translates to only a minor impact on the estimated O abundances. An increase in T_{eff} by $+100$ K typically implies an increase of the derived O by 0.2 dex for the UV OH lines (Nissen et al. 1994). Thus, a new T_{eff}-calibration based on 3D model atmospheres is only expected to introduce a $\lesssim 0.05$ dex alteration of the inferred O abundances. Furthermore, there is no significant metallicity dependence in the T_{eff}-corrections, which could bias any deduced [O/Fe] trends.

We conclude that [O/Fe] determinations will *not* be substantially modified due to changes in the stellar parameters entailed by the adoption of 3D model atmospheres.

5.3. Surface gravity

In addition to a specification of T_{eff} (Sect. 5.2), knowledge of the stellar surface gravity, $\log g$, is required for the spectral synthesis. In Sect. 4 the 3D and 1D calculations were performed with identical $\log g$, which may not be appropriate.

The best method to determine stellar surface gravities is to make use of the accurate parallaxes now available from the
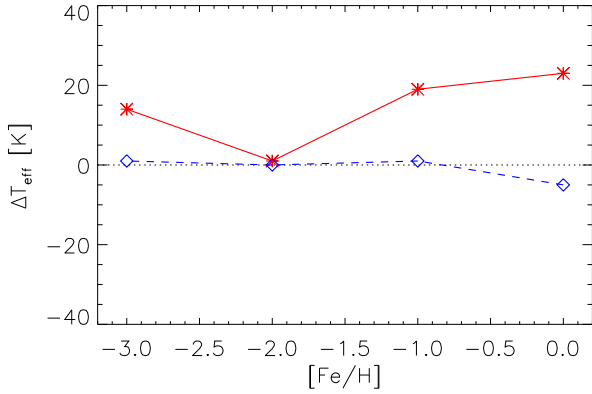
Fig. 5. The differences in $T_{\rm eff}$ derived from IRFM for the solar (solid line) and turn-off (dashed line) sequences of models in the sense $T_{\rm eff,3D}$- $T_{\rm eff,1D}$. The dotted line represent equality between the $T_{\rm eff}$ determinations

Hipparcos mission. By manipulating the familiar relationships $g \propto M/R^2$ and $L \propto R^2 T_{\rm eff}^4$, the trigonometric gravities are:

$$\log g = 4\log T_{\rm eff} + \log M/M_\odot + 2\log\pi + 0.4(V+BC) - 10.51 \quad (1)$$

where M is the stellar mass, V is the apparent visual magnitude of the star corrected for extinction, BC is the bolometric correction and π is the parallax (e.g. Nissen et al. 1997). The additional uncertainty introduced by the use of 3D model atmospheres instead of classical 1D models enters through the small systematic differences in $T_{\rm eff}$ and BC, while the indirect effect on the derived mass through isochrone-fitting is negligible. As seen in Sect. 5.2, the difference in $T_{\rm eff}$-calibration between the two types of models amount to ± 20 K in the relevant temperature range, which corresponds to an error of merely ± 0.01 dex for $\log g$. No bolometric corrections have yet been computed with 3D model atmospheres but considering that $\Delta T_{\rm eff} = 500$ K corresponds to $\Delta BC \simeq 0.05$ for $T_{\rm eff} \simeq 6000$ K with 1D model atmospheres (e.g. Alonso et al. 1995), a very conservative limit to the differential effect of 3D models is $\Delta BC \leq 0.1$. Thus, $\log g$ determinations using 3D model atmospheres are only expected to be ≤ 0.05 dex different from a corresponding 1D analysis when relying on the parallax-method. We emphasize that this is not the full uncertainty with this method, which is dominated by the errors in the parallax measurements and the $T_{\rm eff}$-calibration, but only the additional uncertainty relative to the 1D case when relying on 3D model atmospheres. In terms of derived O abundances, $\Delta \log g \leq \pm 0.05$ corresponds to $\Delta(O/H) \leq \mp 0.02$ dex for the UV OH lines (Nissen et al. 1994). We can therefore safely conclude that our assumption of identical adopted surface gravities in the 3D-1D comparison in Sect. 4 will not impede the conclusions presented therein.

Alternative methods to derive stellar surface gravities are available from spectroscopy, in particular by enforcing ionization equilibrium or using the pressure-damped wings of strong lines. Unfortunately they suffer from several drawbacks which make them less attractive in analyses with 3D model atmospheres. In LTE the 3D abundances derived from Fe I lines are much lower than in classical 1D analyses (Asplund et al. 1999a), which, if correct, would lead to large modifications of the derived $\log g$ from ionization balance. However, the Fe I lines are almost certainly seriously affected by departures from LTE in 3D models, and thus a 3D non-LTE study of Fe line formation would be required, a very challenging task for the future. Indeed, even with 1D model atmospheres departures from LTE make the ionization gravities discrepant from trigonometric gravities (Allende Prieto et al. 1999b, cf. Sect. 5.4). Similarly, the strong lines normally utilised for gravity-determinations are from species which can be expected to be affected by departures from LTE in 3D model atmospheres (Mg I, Ca I, Fe I), again necessitating 3D non-LTE investigations. Furthermore, at very low metallicities ([Fe/H] $\lesssim -2$) also the strongest lines become too weak to accurately probe the photospheric pressure structure (Fuhrmann 1998).

5.4. Metallicity

Stellar metallicities enter into abundance analyses both indirectly through their influence on the photospheric structure and directly through the use of Fe as a reference element for abundance ratios. While the dependence on the former is relatively weak (an error in [Fe/H] as large as 0.4 dex only implies an uncertainty in the derived O abundance from OH lines of 0.05 dex, Nissen et al. 1994), the latter is as important as deriving accurate O abundances when attempting to trace the evolution of [O/Fe]. This obvious fact is, however, often overlooked with values simply taken from the literature or estimated only from Fe I lines with no consideration for departures from LTE. Since the recent analyses of UV OH lines by Israelian et al. (1998) and Boesgaard et al. (1999) have utilised Fe I lines, their derived [O/Fe] trends may be systematically overestimated (King 2000; Israelian et al. 2001), which in turn could influence the 3D-1D comparison presented in Sect. 4. Recently two investigations of non-LTE effects in Fe I line formation in metal-poor stars have been published (Gratton et al. 1999; Thevenin & Idiart 1999) although with discomfortingly discordant results, which deserves further scrutiny.

We tend to view the calculations of Gratton et al. (1999) with some balanced scepticism. Their incomplete treatment of the high-excitation levels, neglect of available quantum mechanical calculations for the photo-ionization cross-sections (from e.g. the IRON Project, Bautista 1997) and their exceedingly large cross-sections for inelastic collisions with H, all combine to ensure a result close to the LTE prediction. Thevenin & Idiart (1999) on the other hand adopt more realistic atomic input data but still suffer from the incomplete handling of the line-blanketing. Since the main non-LTE effect, over-ionization, feeds on the UV radiation field it is paramount to address the UV line-blocking in the calculations of the photo-ionization rates to avoid predicting too large departures from LTE for Fe I. Furthermore, improved quantum mechanical calculations for the H-collisions are urgently needed to replace the questionable classical recipe of Drawin (1968).

Until improved non-LTE calculations are available, we urge that the determinations of stellar Fe abundances to be based

on Fe II lines. Fe II lines are essentially immune to departures from LTE (e.g. Shchukina & Trujillo Bueno 2001) and as clear from Table 3 are not particularly affected by the temperature inhomogeneities and different temperature structures in 3D model atmospheres. At this stage, however, we can not exclude that the estimated [O/Fe] trend with 3D models (Fig. 4) may even need further downward adjustment due to departures from LTE for Fe I lines, on which the existing 1D [Fe/H] estimates are based (Israelian et al. 1998, 2001; Boesgaard et al. 1999). Naturally, investigations of departures from LTE for Fe in metal-poor stars should also be based on the new generation of 3D model atmospheres.

5.5. Molecular equilibrium for OH formation

For the LTE line formation calculations presented in Sect. 4, the assumption of instantaneous molecular equilibrium has been made in the computation of the total number density of OH molecules at different times and locations in the 3D model atmospheres. According to Fig. 1, the OH line formation is strongly biased towards the upflow regions, where the gas is very rapidly cooled from about $10\,000$ K to about 4000 K in a relatively thin zone around continuum optical depth unity. This transition occurs on a time-scale of merely a few minutes for the upflowing material in the Sun, which could imply that molecular equilibrium is not established. Additionally, photodissociation due to the non-local radiation field from deeper layers may cause further departures from LTE. As a result, one would expect that LTE may overestimate the OH content and therefore that the O LTE abundances may be underestimated.

In principle it is a straight-forward exercise to compute the OH molecule formation and the resulting OH number densities as a function of time in our 3D model atmospheres by solving a set of coupled differential equations corresponding to a network of chemical pathways. However, a major obstacle is the apparent lack of rate coefficients for the relevant reactions and temperatures, both experimental and theoretical. We have scoured various publically available databases such as UMIST (Le Teuff et al. 2000) in search of the necessary rate coefficients but with little success in locating data for $T \gtrsim 3000$ K, which prevents us from performing the non-LTE chemistry calculations.

Some guidance to the non-LTE behaviour may still be obtained from observations in the absence of detailed computations. Uitenbroek (2000a,b) has recently concluded from a comparison of the observed solar CO line intensities and their temporal variations with calculations based on both 1D hydrodynamical chromospheric simulations (Carlsson & Stein 1992, 1995, 1997) and 3D model atmospheres similar to those utilised here (Stein & Nordlund 1998) that the inherent assumption of instantaneous molecular equilibrium for CO may not be valid in the Sun. This may suggest that a similar phenomenon could also occur for OH. If so, it would probably be more pronounced in metal-poor stars in view of their more rapid and dramatic cooling in the photosphere.

We conclude that it can not be excluded that departures from molecular equilibrium may influence the derived O abundances when using OH lines and that its magnitude could be metallicity dependent. Naturally this should be examined further once the necessary data becomes available.

5.6. Local thermodynamic equilibrium for OH line formation

Besides the assumption of chemical equilibrium for the OH molecule formation, it should be borne in mind that LTE has also been assumed in the OH line transfer calculations presented in Sect. 4. Due to the vast number of relevant levels and transitions, detailed non-LTE calculations for the OH radiative transfer is formidable. In fact, non-LTE effects for molecules in stellar atmospheres is largely unexplored even with 1D model atmospheres.

We are not aware of any non-LTE studies for OH but CO has attracted slightly more attention. Uitenbroek (2000b) has recently performed detailed non-LTE calculations for the CO vibrational-rotational lines in the Sun, which confirm the insightful prediction by Hinkle & Lambert (1975) that the lines are collisionally controlled and thus that LTE is a good approximation. Hinkle & Lambert caution on the other hand that electronic molecular transitions, like the UV OH lines, may be radiatively determined. If one approximates the UV OH line formation with the two-level approach with complete redistribution (cf. Mihalas 1978), the line source function S_l will depend on the mean intensity averaged over the absorption profile $\bar{J}_\lambda = \int \phi_\lambda J_\lambda d\lambda$ and Planck function $B_\lambda(T)$ as $S_l = (1-\epsilon)\bar{J}_\lambda + \epsilon B_\lambda(T)$. Here ϵ is a measure of the photon destruction probability ($0 \le \epsilon \le 1$). In the UV, $\bar{J}_\lambda$ tend to be larger than $B_\lambda(T)$ for weak lines and therefore $S_l > B_\lambda(T)$. As a consequence, one would expect the OH lines to be weaker with scattering than in LTE, or, equivalently, that the derived O abundance will be underestimated in LTE.

A detailed non-LTE calculation for OH including all the vibrational and rotational levels is unfortunately beyond the scope of the present investigation. But we have nevertheless attempted to estimate the non-LTE corrections to the derived O abundances from the UV OH lines using a two-level OH molecule. Although no doubt unrealistically simplistic to allow accurate quantitative estimates of the non-LTE effects, the approach is still expected to yield qualitatively correct results of the non-LTE behaviour for different stellar parameters. For the purpose, version 2.2 of the statistical equilibrium code MULTI (Carlsson 1986) has been used after some minor modifications to allow treatment of OH molecular lines. The two levels correspond to the OH 313.9 nm transition with the same adopted parameters as for the LTE calculations presented in Sect. 4. Additionally, cross-sections for collisions with electrons and hydrogen must be specified. For the former the classical recipe of van Regemorter (1962) was adopted in the absence of more appropriate treatments. For H-collisions the calculations were performed with the formula by Drawin (1968) multiplied by a variable factor x. It should be noted that the Drawin formula was developed for atoms and it is not clear whether it is at all applicable for molecules. Although often used in non-LTE calculations for late-type stars (cf. discussion in Kiselman 2001),

Table 4. The 1D non-LTE O abundance corrections when using a two-level model-molecule to study the UV OH line formation. The last two 1D models correspond to HD 140283 and G64-12, respectively.

T_{eff} [K]	$\log g$ [cgs]	[Fe/H]	[O/Fe][a] [dex]	x[b]	$\Delta\log\epsilon_{\text{O}}$[c] [dex]
5780	4.44	+0.0	0.0	0.0	+0.18
				0.01	+0.18
				0.1	+0.18
				1.0	+0.17
				10	+0.12
				100	+0.03
5780	4.44	−1.0	+0.4	0.0	+0.20
				0.01	+0.20
				1.0	+0.17
5780	4.44	−2.0	+0.8	0.0	+0.25
				0.01	+0.25
				1.0	+0.22
5780	4.44	−3.0	+1.2	0.0	+0.26
				0.01	+0.26
				1.0	+0.24
				100	+0.04
5690	3.67	−2.5	+0.5	0.0	+0.25
				0.01	+0.25
				1.0	+0.24
			+1.0	0.0	+0.27
				0.01	+0.27
				1.0	+0.26
6450	4.04	−3.0	+1.0	0.0	+0.15
				0.01	+0.15
				1.0	+0.15

[a] The solar O abundance is here assumed to be $\log\epsilon_{\text{O}} = 8.90$
[b] The factor which is multiplied to the Drawin (1968) recipe for the collisional cross-sections with H
[c] The non-LTE O abundance correction defined as $\Delta\log\epsilon_{\text{O}} = \log\epsilon_{\text{O}}^{\text{NLTE}} - \log\epsilon_{\text{O}}^{\text{LTE}}$

evidence is now mounting that the simple-minded approach by Drawin severely overestimates the importance of H-collisions by at least three orders of magnitude for atomic transitions (Fleck et al. 1991; Belyayev et al. 1999). The inclusions of vibrational and rotational sub-levels and line-blanketing in the UV radiation field are also expected to diminish the non-LTE effects due to stronger collisional quenching and decreased $\bar{J}_\lambda/B_\lambda(T)$ ratios in the line-forming region.

Non-LTE calculations have been performed for four 1D model atmospheres with the solar T_{eff} and $\log g$ but different metallicities ([Fe/H] = 0.0, −1.0, −2.0, and −3.0), as well as for selected metal-poor stars (e.g. HD 140283 and G64-12) for different O abundances to estimate the influence of the line strength. In all cases, the effect of H collisions were investigated by computing the abundance corrections for three different x: 0.0, 0.01 and 1.0. The 1D models are not identical to those adopted for the solar sequence in the 3D-1D LTE comparison in order to strictly isolate the metallicity dependence of the non-LTE effects.
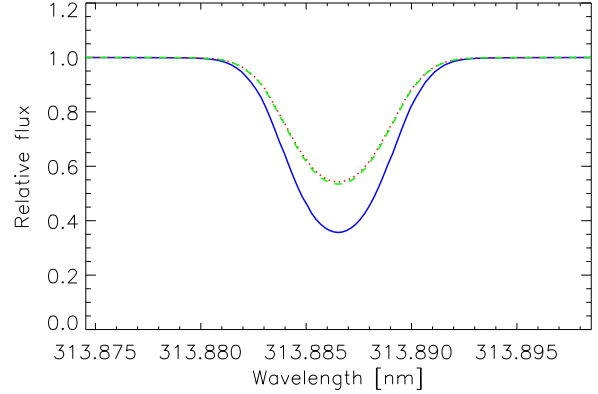

Fig. 6. The 1D OH 313.9 nm line in a metal-poor ([Fe/H] = −3.0) Sun in LTE (solid lines), and in non-LTE with $x = 1.0$ (dashed lines) and $x = 0.0$ (dotted lines), see text for details. Clearly the inclusion of collisions by H according to the Drawin (1968) formula ($x = 1.0$) has a negligible impact on the resulting line strength

A summary of the results in terms of abundance corrections is presented in Table 4. As expected, in all cases the assumption of LTE makes the lines stronger, and therefore that LTE analyses underestimate the O abundances. The difference in terms of line strengths is quite large (Fig. 6) and therefore relatively large non-LTE corrections are obtained, $\simeq 0.2$ dex. The predicted 1D non-LTE effects are almost independent on the stellar parameters. Fortunately, the magnitude of the non-LTE corrections is only marginally dependent on the treatment of the H collisions provided the Drawin (1968) formula does not greatly underestimate the collisional cross-sections ($x > 10$). Even with $x = 1.0$ the predicted non-LTE corrections differ only by ≤ 0.03 dex compared to the case when neglecting the H collisions completely. In all cases, the same results are obtained with $x = 0.01$ and $x = 0.0$. We emphasize though that it is still unclear whether the Drawin recipe can be applied also to molecules. But at this stage there are no indications that the treatment of H collisions play any significant role in the predicted non-LTE corrections.

The departures from LTE in this two-level approach are purely due to scattering in the line, in agreement with the prediction by Hinkle & Lambert (1975) (Fig. 7). Since $\bar{J}_\lambda/B_\lambda(T) > 1$ at the relevant atmospheric layers for the studied model atmospheres, the line source function S_l exceeds the LTE value. This effect is more pronounced in the metal-poor models but its influence on the abundance corrections is partly balanced by the weaker lines at lower metallicities. Since the vast majority of the OH molecules will be in the ground electronic state and the vibrational and rotational levels within electronic states are closely coupled through collisions, the departure coefficient $\beta = N_l/N_l^{\text{LTE}}$ for the lower level will be very close to one and thus no non-LTE effects due to differences in line opacity emerge, as evident from Fig. 7.

In spite of the significant 1D non-LTE abundance corrections, we find no evidence for a pronounced steepening of the
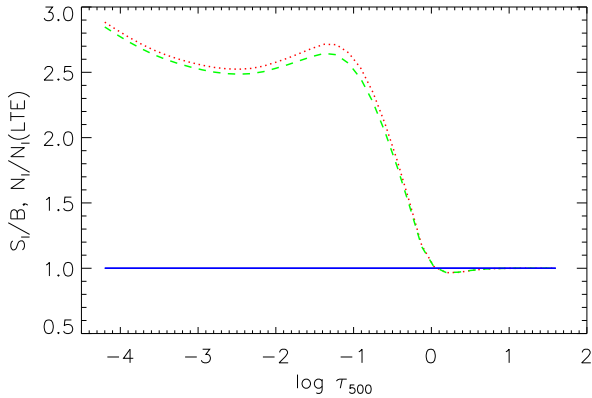
Fig. 7. The ratio of the line source function with the Planck function $S_l/B_\lambda(T)$ for the two cases $x = 1.0$ (dashed lines) and $x = 0.0$ (dotted lines) in a metal-poor ([Fe/H] $= -3.0$) Sun, see text for details. Also shown are the departure coefficients $\beta = N_l/N_l^{\mathrm{LTE}}$ for the lower level of the OH transition for $x = 1.0$ and $x = 0.0$ (solid lines), emphasizing that the non-LTE effect is purely due to scattering and not changes in the line opacity

[O/Fe] trend. However, we caution that this conclusion can not automatically be extrapolated to the 3D case, in which the departures from LTE may be more severe in metal-poor stars since the steep temperature gradients may be more prone to scattering effects than in 1D model atmospheres. Needless to say, an investigation of the non-LTE behaviour in 3D model atmospheres as a function of metallicity has very high priority.

5.7. Summary of uncertainties: 3D or 1D model atmospheres?

Considering that the results presented here are among the first investigations of the impact of the new generation of 3D hydrodynamical model atmospheres on stellar spectroscopy, it is therefore in order to ask if indeed these models are more realistic than previously used classical 1D model atmospheres. Sofar the predictions from the *ab-initio* 3D models have been very successfully confronted with detailed observational constraints for in particular the Sun. These comparisons include such disparate tests as granulation topology and flow field (Stein & Nordlund 1998), helioseismology (Rosenthal et al. 1999), intensity brightness contrast (Stein & Nordlund 1998; Asplund et al. 2000a), flux distribution and limb-darkening (Asplund et al. 1999b) and spectral line shapes, shifts and asymmetries (Asplund et al. 2000b). No doubt the current surface convection simulations for the Sun have a very high degree of realism. In sharp contrast theoretical 1D model atmospheres fail in regards to most, if not all, of the above-mentioned tests. Recently similar 3D models have been used for studies of line asymmetries in Procyon (Allende Prieto et al. 2001) and the metal-poor halo star HD 140283 (Allende Prieto et al. 1999a; Asplund et al., in preparation) with very satisfactory outcomes.

In view of the detailed discussion given in Sect. 5 on possible remaining systematic errors in the 3D analysis, the reader may get the impression that the here presented results are rather uncertain. It may therefore be in order to point out that all of these possible effects also apply equally well to any study based on 1D model atmospheres, besides the errors introduced by the assumption of hydrostatic equilibrium and by treating convection through the mixing length theory (or a close relative thereof), which is known to be a poor representation of stellar convection. However, at this stage it is probably premature to conclude that 3D model atmospheres are indeed superior to classical 1D models. It is therefore of utmost importance now to carry out the same arsenal of tests which previously has been undertaken with 1D model atmospheres (flux distribution, limb-darkening, colours, H-lines etc) as well as additional ones now possible (line asymmetries and shifts, asteroseismology), in particular for metal-poor stars. This is even more true in light of the fact that 1D model atmospheres often fail the very same tests.

6. Comparing previous OH, O I and [O I] results

Even if the present article does not deal directly with observations, in this section we will nevertheless discuss some of the recent analyses of various O diagnostics as it has bearing on our findings and may give clues to the existence or not of the large granulation corrections for OH in metal-poor stars described in Sect. 4.

A major argument for the monotonic linear trend in [O/Fe] with metallicity derived from the UV OH lines comes from the claimed good agreement with the O I triplet results (Israelian et al. 1998, 2001; Boesgaard et al. 1999). Since much smaller granulation corrections are expected for the triplet than for OH (Asplund 2001) this would seem to contradict the findings in Sect. 4. However, the consonance between the OH and O I results is not as unambigous when examining some of the published analyses in detail. Fig. 8 shows the difference between the OH-based and O I-based abundances of Boesgaard et al. (1999) on the King (1993) T_{eff}-scale; with the lower Carney (1983) scale the correlation is slightly less pronounced but clearly present (slope $= -0.13$ instead of -0.18). The absolute value for the abundance differences is here less important than the existence of the metallicity-trend due to the uncertainty introduced by the choice of T_{eff}-scale and the neglect of non-LTE effects for O I. This divergent behaviour is very close to the expected according to the results of Sect. 4 and Asplund (2001), which we interpret as a qualitative argument for the aptness of the 3D calculations. In view of this, the good general agreement found by Israelian et al. (1998) for nine stars using the O I equivalent widths of Tomkin et al. (1992) pose a perplexing problem. Clearly a larger stellar sample with simultaneous analyses of the OH and O I lines would be very helpful in this context. One should also explore possible differences in for example C abundances derived from C I and CH lines at low metallicities. Preliminary calculations reveal significant but smaller differences between 1D and 3D analyses of CH lines compared with for OH lines (≈ 0.3 dex instead of ≈ 0.6 dex for OH at [Fe/H] $= -3.0$).
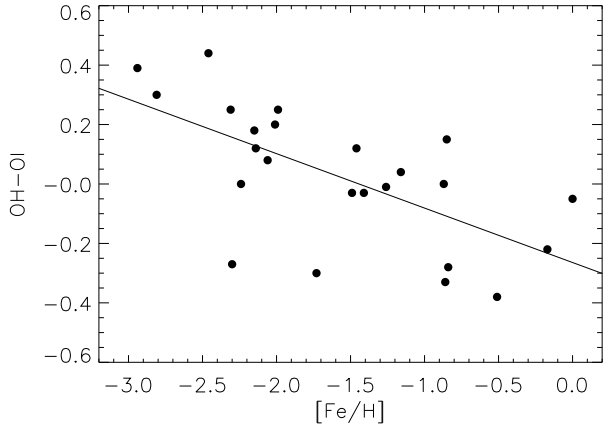
Fig. 8. The difference between the OH and O I-based 1D abundances of Boesgaard et al. (1999) on the King (1993) $T_{\rm eff}$-scale, which reveals a pronounced metallicity-dependent trend (slope -0.18). This behaviour is in qualitative agreement with the 3D calculations presented in Sect. 4

The conventional [O/Fe] plateau indicated by the [O I] line has recently received support from the IR OH vibrational-rotational lines (Balachandran et al. 2001; Melendez et al. 2001). As discussed in Sect. 4, this could be interpreted as the here presented granulation corrections for the UV OH lines in metal-poor stars are overestimated, since for the same star the IR and UV lines should to first order be affected similarly (with the possible exception of non-LTE effects in the line formation, cf. Sect. 5.6). A more likely explanation in our opinion, however, is to be found in the differences in stellar parameters, in particular $T_{\rm eff}$, for the sofar investigated UV and IR targets. As evident from Table 2 and Fig. 3, the magnitude of the OH granulation corrections depend on $T_{\rm eff}$ in the sense that larger effects are present for higher temperatures. Although dangerous to extrapolate, we speculate that significantly smaller OH abundance corrections than found here will be obtained for $T_{\rm eff} \lesssim 5000\,{\rm K}$, which is typical for the metal-poor stars with detected IR OH features. The physical reason for the dependence on $T_{\rm eff}$ is the strength of the coupling between the gas and radiation field: for lower $T_{\rm eff}$, more and stronger spectral lines are available which contribute additional radiative heating, keeping the gas temperature closer to the radiative equilibrium value (Asplund et al., in preparation). No 3D model atmospheres are yet available for these lower $T_{\rm eff}$ which prevent verification of our hypothesis but such convection simulations are currently being constructed.

Due to the inconspicous nature of the [O I] line (Nissen et al. 2001), no direct comparison with the UV OH results has sofar been possible for metal-poor dwarfs with [Fe/H] < -2. Recently, Fulbright & Kraft (1999) have considered the [O I] line in the two metal-poor ([Fe/H] $\lesssim -2.1$) subgiants BD+23°3130 and BD+37°1458 ($T_{\rm eff} = 5130\,{\rm K}$ and $5260\,{\rm K}$, respectively), which have been re-analysed by Israelian et al. (2001). The UV OH lines suggest [O/Fe] = 0.60 and 0.50, respectively, in the two stars, i.e. in significantly better agreement

with the traditional [O/Fe] plateau compared with the linear trend seemingly implied by the OH lines in the hotter stars. As for the IR analyses, we conjecture that at $T_{\rm eff} \simeq 5200\,{\rm K}$ significantly smaller granulation corrections than those given in Sect. 4 will be deduced, leaving the plateau-like [O/Fe] ratios largely unchallenged. Excellent agreement between [O I] and OH is found for both stars: the forbidden line gives [O/Fe] = 0.62 and 0.52, respectively. The latter values come from our own analysis using 1D MARCS model atmospheres with the stellar parameters given in Israelian et al. (2001). The equivalent widths for [O I] and Fe II were taken from Fulbright & Kraft except for [O I] in BD+23°3130 for which we relied on the VLT-measurement ($W_\lambda = 0.15\,{\rm pm}$) by Cayrel (2001). This [O/Fe] estimate for BD+23°3130 is for unknown reason significantly lower than reported in Israelian et al. (2001), [O/Fe] = 0.82, while in perfect agreement with the findings of Balachandran (2001, private communication) using Kurucz (1993) model atmospheres but otherwise identical input.

7. Concluding remarks

The low atmospheric temperatures encountered in the new generation of 3D hydrodynamical model atmospheres (Asplund et al. 1999a, 2000a,b, Allende Prieto et al. 2001; Asplund et al., in preparation) compared with classical 1D hydrostatic model atmospheres for metal-poor stars have a profound impact on the OH line formation, as described in Sect. 4. As a consequence, a possible severe systematic error in recent 1D LTE analyses of OH lines in metal-poor stars (Israelian et al. 1998, 2001; Boesgaard et al. 1999) has been exposed, making the case for a monotonic increase in [O/Fe] towards lower metallicities less convincing. Taken at face value, our 3D LTE OH analysis results in [O/Fe] values in rough agreement with the conventional [O/Fe] plateau for [Fe/H] $\lesssim -1$ indicated by the [O I] lines (Fig. 4). We emphasize though that this apparant concordance should not be taken too literally in view of the preliminary nature of our 3D calculations and that no star-by-star comparison has been made with observations. By investigating possible systematic errors for the 3D LTE results it has been found, however, that the conclusion of large granulation effects on the OH lines appears reasonably robust. For example, $T_{\rm eff}$-calibrations using 3D model atmospheres should not differ significantly ($\Delta T_{\rm eff} \lesssim 20\,{\rm K}$) from previous 1D calibrations provided they are based on IRFM; the same is not necessarily true for alternative calibrations using Balmer lines or colours. Similarly, estimates of $\log g$ and [Fe/H] should remain essentially unaltered when relying on Hipparcos parallaxes and Fe II lines. The major remaining uncertainties in the 3D analysis appear to be the assumptions of LTE for the molecular equilibrium and in the line formation. Although not yet investigated for 3D model atmospheres, it is possible that such departures from LTE may indeed steepen the [O/Fe] trend once again but unlikely as much as the original 1D LTE case. On the other hand, departures from LTE for Fe I may diminish the slope further. A final verdict on this issue must therefore await detailed and improved non-LTE calculations. But we note in the meantime that even in the presence of possible non-LTE effects for

OH and Fe I, [O/Fe] ratios will be less affected since both the O and Fe LTE abundances will tend to be underestimated.

The purpose of the present paper has not been to advocate a specific [O/Fe] trend with metallicity since our investigation has been limited to a differential 3D-1D comparison without involving observational confrontation. Nevertheless, our findings will likely fuel the long-standing debate on the O abundances in metal-poor stars. As already stated several times, it would be premature to conclude from our analysis that the monotonic linear trend in [O/Fe] claimed by Israelian et al. (1998, 2001) and Boesgaard et al. (1999) must now be abandoned, even if the arguments for continuously increasing [O/Fe] ratios towards lower metallicities appear much weaker. It should be remembered that many, albeit not all, studies of the O I triplet at 777 nm in dwarfs and subgiants find [O/Fe] values systematically higher than those given by the [O I] line in metal-poor giants and subgiants. The triplet is unfortunately sensitive to the adopted T_{eff}-scale and departures from LTE, which deserve very careful treatment. For the moment, the most reliable [O/Fe] ratios still appear to come from the [O I] line, provided that very high S/N spectra are utilised and the metallicities are estimated from Fe II lines (Nissen et al. 2001; Lambert 2001).

To ignore the existing systematic errors in traditional 1D LTE analyses of the UV OH lines in the hope that departures from LTE in the molecule formation and radiative transfer will conspire to exactly compensate the effects of the low atmospheric temperatures in 3D is certainly fraught with danger and furthermore most likely misleading. As demonstrated above, in order to derive reliable oxygen abundances in very metal-poor stars, unfortunately there is no easier escape route but to perform time-dependent non-LTE calculations in 3D model atmospheres for OH. Fortunately, recent improvements in the analysis of stellar spectra ensure such studies in fact being tractable tasks for the near future, which should help remove many of the lingering uncertainties in the derived oxygen abundances and perhaps finally settle the long-standing debate on [O/Fe] in metal-poor stars.

References

Abia C., Rebolo R., 1989, ApJ 347, 186

Allende Prieto C., Asplund M., García López R.J., Lambert D.L., 2001, submitted to ApJ

Allende Prieto C., Asplund M., García López R.J., Gustafsson B., Lambert D.L., 1999a, in: Theory and tests of convection in stellar structure, ASP conf. series 173, A. Gimenez, E.F. Guinan and B. Montesinos (eds.), p. 205

Allende Prieto C., García López R.J., Lambert D.L., Gustafsson B., 1999b, ApJ 527, 879

Alonso A., Arribas S., Martinez-Roger C., 1995, A&A 297, 197

Asplund M., 2000a, A&A 359, 755

Asplund M., 2000b, in: The light elements and their evolution, da Silva L., Spite M., de Medeiros J.R. (eds.). IAU symposium 198, p. 448

Asplund M., 2001, in: Highlights of Astronomy, IAU, Barbuy B. (ed.), in press

Asplund M., Carlsson M., 2001, submitted to A&A

Asplund M., Gustafsson B., Kiselman D., Eriksson K., 1997, A&A 318, 521

Asplund M., Nordlund Å., Trampedach R., Stein R.F., 1999a, A&A 346, L17

Asplund M., Nordlund Å., Trampedach R., 1999b, in: Theory and tests of convection in stellar structure, ASP conf. series 173, A. Gimenez, E.F. Guinan and B. Montesinos (eds.), p. 221

Asplund M., Ludwig H.-G., Nordlund Å., Stein R.F., 2000a, A&A 359, 669

Asplund M., Nordlund Å., Trampedach R., Allende Prieto C., Stein R.F., 2000b, A&A 359, 729

Asplund M., Nordlund Å., Trampedach R., Stein R.F., 2000c, A&A 359, 743

Balachandran S.C., Bell R.A., 1998, Nature 392, 23

Balachandran S.C., Carr J.S., Carney B.W., 2001, New Astronomy Reviews, in press

Barbuy B., 1988, A&A 191, 121

Bautista M.A., 1997, A&AS 122, 167

Bell R.A., Balachandran S.C., Bautista M.A., 2001, ApJ 546, L46

Belyayev A., Grosser J.J.H., Menzel T., 1999, Phys. Rev. A 60, 2150

Bessell M.S., Hughes S.M.G., Cottrell P.L., 1984, PASA 5, 547

Bessell M.S., Sutherland R.S., Ruan K., 1991, ApJ 383, L71

Blackwell D.E., Shallis M.J., 1977, MNRAS 180, 177

Boesgaard A.M., King J.R., Deliyannis C.P., Vogt S., 1999 AJ 117, 492

Carlsson M., 1986, Uppsala Astronomical Observatory Report No. 33

Carlsson M., Stein R.F., 1992, ApJ 397, 59

Carlsson M., Stein R.F., 1995, ApJL 440, 29

Carlsson M., Stein R.F., 1997, ApJ 481, 500

Carney B.W., 1983, AJ 83, 623

Carretta E., Gratton R.G., Sneden C., 2000, A&A 356, 238

Cayrel R., 2001, New Astronomy Reviews, in press

Conti P.S., Greenstein J.L., Spinrad H., Wallerstein G., Vardya M.S., 1967, ApJ 148, 105

Drawin H.W., 1968, Z. Physik 211, 404

Fleck I., Grosser J., Schnecke A., Steen W., Voigt H., 1991, JPhysB 24, 4017

Freytag B., Ludwig H.-G., Steffen M., 1999, in: Theory and tests of convection in stellar structure, Gimenez A., Guinan E.F., Montesinos B. (eds). ASP conference series 173, p. 225

Fulbright J.P., Kraft R.P., 1999, AJ 118, 527

Fuhrmann K., 1998, A&A 330, 626

Gratton R.G., Carretta E., Eriksson K., Gustafsson B., 1999, A&A 350, 955

Grevesse N., Sauval A.J., 1998, in: Solar composition and its evolution – from core to corona, Frölich C., Huber M.C.E., Solanki S.K., von Steiger R. (eds). Kluwer, Dordrecht, p. 161

Gustafsson B., Bell R.A., Eriksson K., Nordlund Å., 1975, ApJ 42, 407

Hinkle K.H., Lambert D.L., 1975, MNRAS 170, 447

Holweger H., Müller E.A., 1974, Solar Physics 39, 19

Israelian G., García López R.J., Rebolo R., 1998, ApJ 507, 805

Israelian G., Rebolo R., García López R.J., et al., 2001, ApJ, in press (astro-ph/0101032)

Karlsson T., Gustafsson B., 2001, submitted to A&A

King J.R., 1993, AJ 106, 1206

King J.R., 2000, AJ 120, 1056

Kiselman D., 2001, New Astronomy Reviews, in press (astro-ph/0010300)

Kiselman D., Nordlund Å., 1995, A&A 302, 578

Kurucz R.L., 1993, CD-ROM, private communication

Lambert D.L., 2001, in: Highlights of Astronomy, IAU, Barbuy B. (ed.), in press

Langer G.E., Hoffman R., Zaidins C.S., 1997, PASP 109, 244

Le Teuff Y.H., Millar T.J., Markwick A.J., 2000, A&AS 146, 157

Ludwig H.-G., Freytag B., Steffen M., 1999, A&A 346, 111

Meléndez J., Barbuy B., Spite F., 2001, submitted to ApJ

Mihalas D., 1978, Stellar atmospheres, W.H. Freeman and Company, San Fransisco

Mihalas D., Däppen W., Hummer D.G., 1988, ApJ 331, 815

Nissen P.E., Gustafsson B., Edvardsson B., Gilmore G., 1994, A&A 285, 440

Nissen P.E., Asplund M., Hill V., D'Odorico S., 2000, A&A 357, L49

Nissen P.E., Primas F., Asplund M., 2001, New Astronomy Reviews, in press

Nordlund Å., 1982, A&A 107, 1

Nordlund Å., Dravins D., 1990, A&A 228, 155

Primas F., Asplund M., Nissen P.E., Hill V., 2000, A&A, 364, L42

Rosenthal C.S., Christensen-Dalsgaard J., Nordlund Å., Stein R.F., Trampedach R., 1999, A&A 351, 689

Shchukina N., Trujillo Bueno J., 2001, ApJ, in press

Sneden C., Kraft R.P., Prosser C.F., Langer G.E., 1991, AJ 102, 2001

Stein R.F., Nordlund Å., 1998, ApJ 499, 914

Thevenin F., Idiart T., 1999, ApJ 521, 753

Uitenbroek H., 2000a, ApJ 531, 571

Uitenbroek H., 2000b, ApJ 536, 481

VandenBerg D.A., Bell R.A., 2001, New Astronomy Reviews, in press

van Regemorter H., 1962, ApJ 136, 906